

RESEARCH

Open Access



# Constant envelope OFDM RadCom fusion system

Yixuan Huang<sup>1</sup>, Su Hu<sup>1\*</sup> , Shiyong Ma<sup>1</sup>, Qu Luo<sup>1</sup>, Dan Huang<sup>1</sup>, Yuan Gao<sup>2,3</sup> and Rong Shi<sup>4</sup>

## Abstract

A joint radar and wireless communication (RadCom) fusion system is an important trend for future intelligent transportation, such as the Internet of Vehicles (IOV). However, traditional joint orthogonal frequency division multiplexing (OFDM)-based RadCom fusion system suffers from the problem of high peak-to-average power ratio (PAPR) of transmission signals, leading to nonlinear distortion in high power amplifiers (HPAs). To solve this problem, a new constant envelope OFDM RadCom approach is proposed in this paper. Taking phase modulation into consideration, the constant envelope OFDM RadCom system obtains 0 dB PAPR value, which results in linear high power amplifier being feasible. In the receiver side, both communication transmission and target detection are guaranteed by a phase demodulator and frequency-domain signal processing algorithm, respectively. Simulation results demonstrate that the constant envelope OFDM RadCom system is a feasible solution for future IOV with the capability of target detection and wireless communication simultaneously.

**Keywords:** Constant envelope, Radar, Wireless communication, OFDM

## 1 Introduction

For future Internet of Vehicles (IOV) systems, all vehicles adopt both wireless communication and radar equipment in order to improve the safety of its drivers [1]. In a modern vehicle, the communication equipment is used to receive radio signals and the radar equipment is used for the short-distance warning. To avoid interference between the communication system and radar system, the spectrum has to be different. Therefore, it results in wasting frequency spectrum resources. Consequently, it is necessary to complete joint communication and radar function in a fusion system within the same frequency spectrum [2]. Such fusion systems, providing radar and communication functions on a single hardware platform with a single waveform, will be denoted in the following with the acronym “RadCom” [1, 2].

Recalling from traditional wireless communication and radar systems, typical radar signals are immovable, whereas traditional wireless communication signal is random due to data-driving transmitting signals. Taking spectrum efficiency and hardware cost into consideration, a unique fusion system consists of wireless

communication and radar application, which accomplishes the essential tasks of environmental sensing and information transmission. Till now, RadCom fusion systems become recently an important trend for communication and radar technique development [3]. With such a suitable RadCom system, all vehicles on the road could interact in a cooperative communication and radar fusion network. In Fig. 1, the vehicle with RadCom system could finish information transmission and target detection simultaneously to promote the transportation safety. In addition, RadCom system can be applied in other scenarios like aeronautics and military.

Single-carrier RadCom signals, in combination with spread-spectrum techniques, can be used for multiple-user communication [4–6], whereas its dynamic range remains limited for radar measurements [1]. For multicarrier RadCom waveforms, an additional multiple-access technique is required for multiple-user communication operation [7], and dedicated frequency-domain processing techniques can be exploited to improve the performance of the radar application. In terms of broadband continuous waveform, orthogonal frequency division multiplexing (OFDM) is the key technology of Long-Term Evolution (LTE) and its performance can be promoted by encoding, e.g., the turbo code [8, 9].

\* Correspondence: [husu@uestc.edu.cn](mailto:husu@uestc.edu.cn)

<sup>1</sup>University of Electronic Science and Technology of China, Chengdu, China  
Full list of author information is available at the end of the article

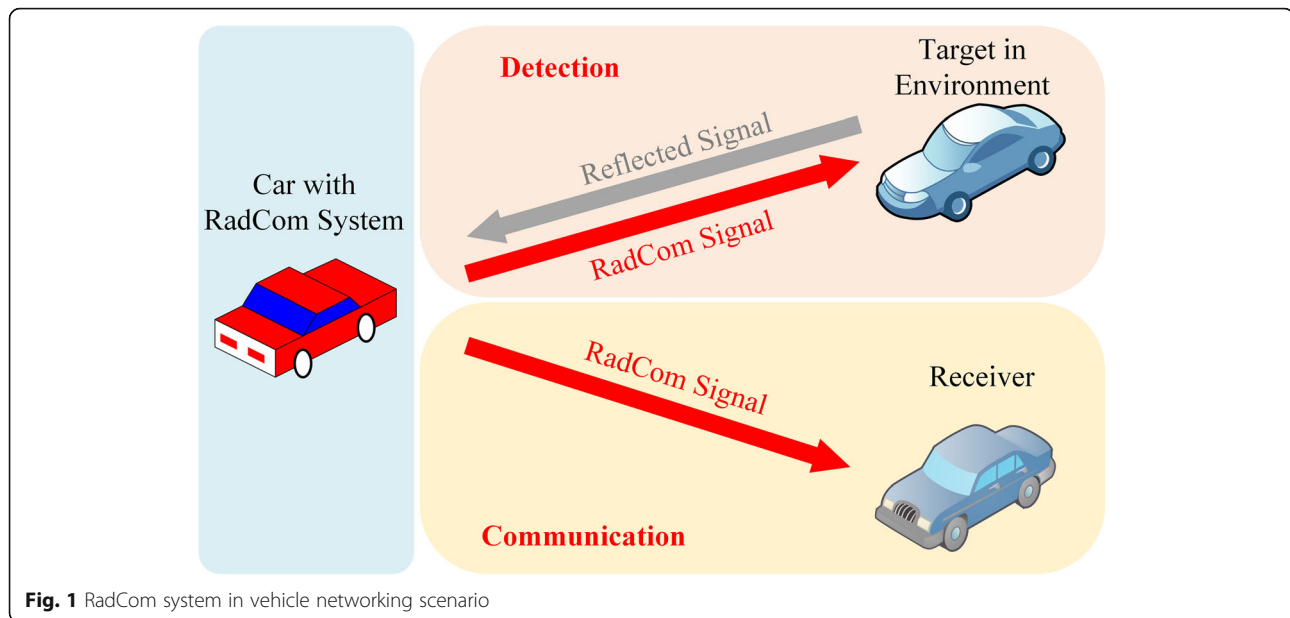


**Fig. 1** RadCom system in vehicle networking scenario

Channel estimation is the key process of multicarrier systems [10]. For the application of multicarrier waveforms and frequency-domain modulation, frequency-domain equalization (FDE) can be used in multicarrier systems, and the complexity of channel estimation is reduced effectively. However, the peak-to-average power ratio (PAPR) of traditional OFDM signals can be bigger than 7 dB, which is a rough index for the high power amplifier (HPA). In radio frequency front end, the efficiency of HPA is degenerated with increasing PAPR of input signals [11–13]. The high PAPR value of OFDM signals will lead to the serious nonlinear distortion of HPAs [14–16]. As a consequence, it is significant to decrease PAPR of OFDM transmitting signals for engineering practical applications.

In this paper, a new constant envelope OFDM (CE-OFDM) RadCom system is proposed. This system can provide radar and wireless communication functions simultaneously. The PAPR of CE-OFDM is 0 dB. In this article, both the phase modulator and the phase unwrap demodulator guarantee constant envelope communication signals [17, 18]. A unique frequency-domain processing algorithm ensures target information is obtained [19–21]. The constant amplitude of CE-OFDM RadCom signals means that the common HPAs can satisfy the requirement for transmitting signals, and the OFDM high PAPR problem can be perfectly solved.

Ambiguity function is an evaluation standard for RadCom system, which is a cross field of communication and radar. The characteristic of signal energy concentration in time-frequency domain can be obtained by its ambiguity function. The characteristic of signal energy concentration has an effect on inter-symbol

interference (ISI) and inter-carrier interference (ICI) in communication systems. The ambiguity function is also useful for investigating different radar waveforms and determining the range and Doppler resolution of the special waveform [22]. Observing the ambiguity function of signals, the signal characteristic, which not only includes the orthogonality and energy distribution of communication signals but also contains delay ambiguity and Doppler ambiguity of radar signals, can be obtained. In this paper, ambiguity function analysis of CE-OFDM RadCom signals is provided.

This paper is organized as follows: Section 2 presents the CE-OFDM RadCom fusion approach. Section 3 and Section 4 describe the CE-OFDM RadCom communication analysis and the frequency-domain detection algorithm, respectively. The simulation method is introduced in Section 5. In Section 6 and Section 7, comprehensive simulation and analysis are presented, including bit error rate (BER) performance, ambiguity analysis, multiple target detection, detection threshold, and detection probability. Conclusions are presented in Section 8.

## 2 CE-OFDM multi-carrier RadCom systems

With the capability of wireless communication and target detection, some applications can benefit from the RadCom fusion systems, such as intelligent transportation applications. With a suitable RadCom system, all vehicles on the road could interact in an integrated radar and communication sensor network, which promotes transportation security. Therefore, the key of RadCom development is to design waveforms that are suitable for both wireless communications and radar functions [1, 2].

Compared with traditional OFDM system, the key of CE-OFDM system is to solve OFDM high PAPR problem effectively. This section principally introduces a new CE-OFDM multi-carrier RadCom fusion approach. The constant envelope RadCom fusion approach is based on the CE-OFDM system, in which the real-valued OFDM signals are modulated by a phase modulator to obtain constant amplitude signals. For promoting spectral effectiveness, the frequency-domain detection algorithm is combined in this fusion approach to ensure the real-time environment sensing detection. The CE-OFDM RadCom fusion approach is able to accomplish environment detection and wireless communication simultaneously with the same CE-OFDM transmitted signals. Straightforward, this fusion approach makes the continuous CE-OFDM system append detection function within the same time-frequency resources. What is more, CE-OFDM RadCom fusion approach can be implemented by common HPA, and this is helpful for saving hardware cost.

Figure 2 represents CE-OFDM RadCom system architecture. During each  $T$ -second elementary symbol interval, after a quadrature amplitude modulation (QAM) modulator, the bit information is modulated into  $M_{QAM}$ -ary QAM symbols. And then, to make the output of inverse discrete Fourier transform (IDFT) real-valued, QAM symbols are rearranged. For obtaining real-valued OFDM signals  $\{x[n]\}$ , the input of  $N_{DFT}$ -point IDFT is a special data vector [23], which is conjugate symmetric and zero-padded

$$\{0, X[1], X[2], \dots, X[N_{QAM}], \mathbf{0}_{1 \times N_{ZP}}, 0, X^*[N_{QAM}], \dots, X^*[2], X^*[1]\}, \quad (1)$$

where  $\{X[k]\}_{k=1}^{N_{QAM}}$  are  $M_{QAM}$ -ary QAM symbols and  $\mathbf{0}_{1 \times N_{ZP}}$  is a row vector composed of  $N_{ZP}$  zeros.  $N_{DFT} = 2N_{QAM} + N_{ZP} + 2$  is the IDFT size.  $J = N_{DFT}/(N_{DFT} - N_{ZP})$  is the oversampling multiple. The two zeros at index  $k = 0$  and  $k = N_{QAM} + N_{ZP} + 1$  are used to ensure implementation for conjugate symmetry, and the remaining zeros guarantee the result of oversampling the time-domain

sequence. Therefore, the output of the IDFT can be represented as

$$x[n] = \sum_{k=0}^{N_{DFT}-1} X[k] e^{j2\pi kn/N_{DFT}} = 2 \sum_{k=1}^{N_{QAM}} \left\{ \Re\{X[k]\} \cos\left(\frac{2\pi kn}{N_{DFT}}\right) - \Im\{X[k]\} \sin\left(\frac{2\pi kn}{N_{DFT}}\right) \right\}, \quad (2)$$

$n = 0, 1, \dots, N_{DFT} - 1$ , where  $j = \sqrt{-1}$ . For analysis, the continuous time form of  $x[n]$  can be expressed as

$$x(t) = 2 \sum_{k=1}^{N_{QAM}} \left\{ \Re\{X[k]\} \cos\left(\frac{2\pi kt}{T}\right) - \Im\{X[k]\} \sin\left(\frac{2\pi kt}{T}\right) \right\} = 2 \sum_{k=1}^{2N_{QAM}} I[k] q_k(t), \quad (3)$$

$-T_{CP} \leq t < T$ . Where  $T_{CP}$  is the cyclic prefix duration. It is clear that the OFDM signal is comprised of  $N = 2N_{QAM}$  subcarriers. And the symbols on subcarriers are  $M = \sqrt{M_{QAM}}$ -pulse amplitude modulation (PAM) data symbols. Therefore,

$$I[k] = \begin{cases} \Re\{X[k]\}, & k = 1, 2, \dots, N_{QAM} \\ -\Im\{X[k - N_{QAM}]\}, & k = N_{QAM} + 1, \dots, N \end{cases}, \quad (4)$$

$I[k] \in \{\pm 1, \pm 3, \dots, \pm(M - 1)\}$ , and the subcarrier can be written as

$$q_k(t) = \begin{cases} \cos\left(\frac{2\pi kt}{T}\right), & k = 1, 2, \dots, N_{QAM} \\ \sin\left(\frac{2\pi [k - N_{QAM}] t}{T}\right), & k = N_{QAM} + 1, \dots, N \end{cases}. \quad (5)$$

So, the subcarrier orthogonality condition holds:

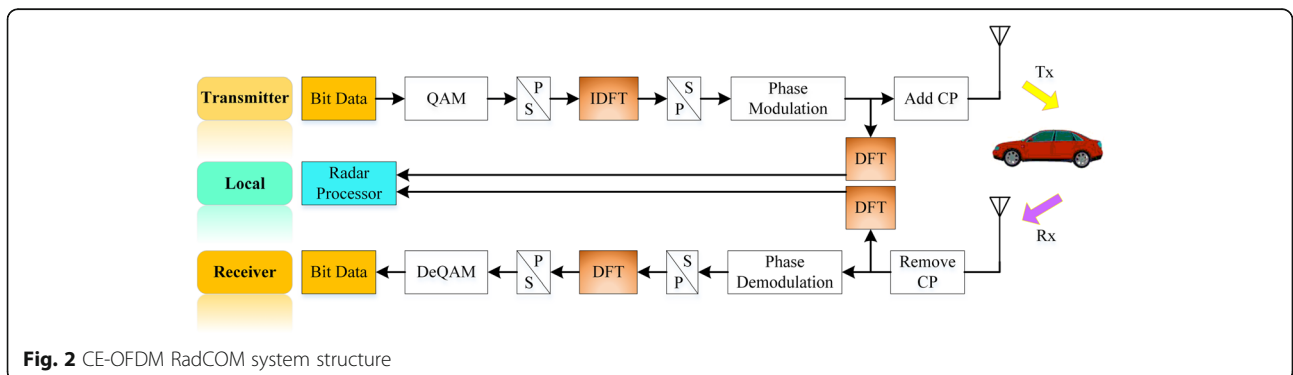


Fig. 2 CE-OFDM RadCOM system structure

$$\int_{iT}^{(i+1)T} q_{k_1}(t-iT)q_{k_2}(t-iT)dt = \begin{cases} T/2, & k_1 = k_2 \\ 0, & k_1 \neq k_2 \end{cases} \quad (6)$$

Next, a phase modulator transforms the high PAPR real-valued OFDM sequence  $\{x[n]\}$  into the constant envelope sequence  $\{s[n] = \exp(jCx[n])\}$ , where  $C$  is a scaling constant. Then, to avoid ISI, an  $N_{CP}$  points cyclic prefix (CP) is needed to obtain  $\{s[n]\}_{n=-N_{CP}}^{N_{DFST}-1}$ , where  $s[n] = s[N_{DFST} + n]$ ,  $n = -N_{CP}, \dots, -2, -1$ . The discrete-time constant envelope samples are then passed through a digital-to-analog converter to obtain the continuous signal. Last, the continuous signal is amplified by HPA and transmitted into the channel.

The modulation index is  $h$ . The phase of CE-OFDM signal is defined as  $\phi[n] = 2\pi h C_{norm} x[n]$ , where  $C_{norm}$  is a constant. To make the variance of phases of CE-OFDM signals  $\sigma_\phi^2 = (2\pi h)^2$ ,  $C_{norm}$  should be set as  $\sqrt{2/(N\sigma_{PAM}^2)}$ , where  $\sigma_{PAM}^2 = (M^2-1)/3$  is the variance of the independent and identically distributed M-PAM symbols. Therefore, the low-pass equivalent representation of the discrete transmitted CE-OFDM signal can be written as

$$\begin{aligned} s[n] &= A \exp\{\phi[n] + \theta\} \\ &= A \exp\{j[2\pi h C_{norm} x[n] + \theta]\}, \end{aligned} \quad (7)$$

$-N_{CP} \leq n < N_{DFST}$  where  $A$  is the signal amplitude and  $\theta$  is an arbitrary phase offset (PO), and it could be used to achieve continuous phase modulation (CPM) [24].

Figure 3 represents the constellation maps of CE-OFDM and OFDM random time-domain signals. The

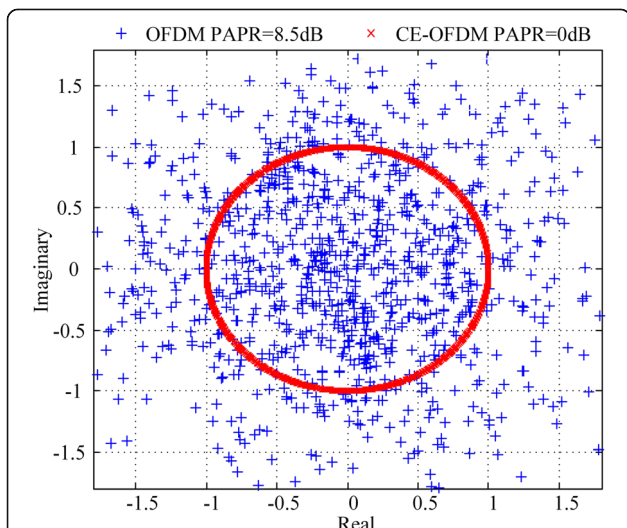


**Fig. 3** Constellation diagram of OFDM and CE-OFDM random signals. Detailed legends: the plus sign represents the OFDM signals with 8.5 dB PAPR, and the cross represents the CE-OFDM signals

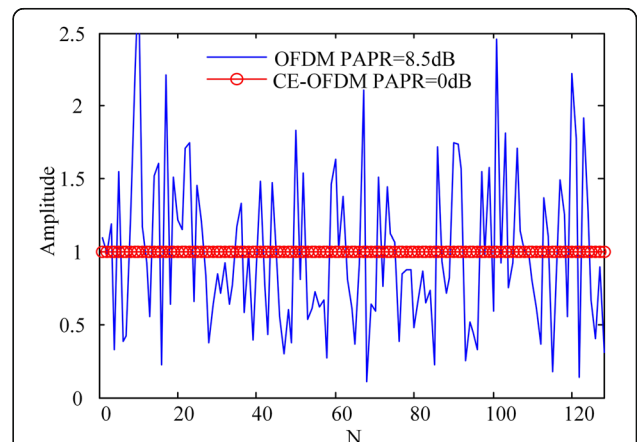
constellation points of OFDM with 8.5 dB PAPR (the plus sign) distribute randomly in its constellation map. Meanwhile, the distance from the constellation points of CE-OFDM (the cross) to zero is constant one, and the CE-OFDM constellation points seem to form a unit circle.

Figure 4 represents amplitude comparison between CE-OFDM time-domain signals and OFDM time-domain signals. The OFDM amplitude distribution is chaotic with 8.5 dB PAPR, and it approximately follows independent random distribution. However, the nonlinear distortion of HPAs, which is caused by high PAPR, could reduce the HPA efficiency [14, 25]. Figure 2 presents that the CE-OFDM amplitude is constant, which means that the requirement of transmitting information can be satisfied by using common HPAs, and the high PAPR problem of traditional OFDM can also be solved [26, 27]. Furthermore, the constant envelope enhances transmission range. Therefore, taking the PAPR problem into consideration, CE-OFDM waveform is one applicable RadCom system candidate.

The envelope of CE-OFDM RadCom transmitted signals is constant, and the nonlinear distortion of HPAs will be eliminated. Consequently, the problem of high PAPR problem of OFDM is saved. The information demodulation and environment sensing are accomplished in the CE-OFDM RadCom receiver. Later on, the information demodulation and performance analysis for wireless communication is represented in Section 3 and the frequency-domain detection process is introduced in Section 4.

### 3 The CE-OFDM RadCom analysis in communication

Since the constant envelope transmitted signals are the result of phase modulation, the bandwidth of  $s(t)$ , which is the continuous signal of  $s[n]$ , is a function of the modulation index. Since the baseband subcarrier signals



**Fig. 4** Amplitude diagram of random signals of OFDM and CE-OFDM. Detailed legend: the line represents the OFDM signals with 8.5 dB PAPR and the line with a circle represents the CE-OFDM signals

are centered at the frequencies  $\pm nT$  Hz,  $n = 1, \dots, N/2$ , the double-sided bandwidth is defined as  $W \equiv N/T$  Hz. The root mean square (RMS) bandwidth of CE-OFDM signals can be defined as [28]

$$B = \max(2\pi h, 1)W \text{ Hz}, \tag{8}$$

and the bit rate is  $R = N_{QAM} \log_2 \sqrt{M}/T$  bps.

The received communication signal is  $r(t) = \int_0^{\tau_{\max}} h(\tau) s(t - \tau) d\tau + \omega(t)$ , where  $h(\tau)$  is the channel impulse response,  $\tau_{\max}$  is maximum propagation delay, and  $\omega(t)$  is complex-valued additive white Gaussian noise (AWGN) with a power density spectrum  $\Phi_\omega(f) = N_0$ . Provided that the channel with  $L$  paths is static in  $T$  seconds, the received samples are represented as

$$r[n] = \sum_{l=0}^{L-1} h[l]s[n-l] + \omega[n], n = -N_{CP}, \dots, N_{DFT}-1, \tag{9}$$

where  $h[l], s[n]$ , and  $\omega[n]$  represent the discrete time samples of channel impulse response, CE-OFDM signals, and AWGN, respectively. The CP duration is fixed according to  $N_{CP} \geq L$ . Therefore,  $r[n]$  could be rewritten as

$$r[n] = \begin{cases} s[n] * h[n] + \omega[n], & n = -N_{CP}, \dots, N_{DFT}-1 \\ s[n] \odot h[n] + \omega[n], & n = 0, \dots, N_{DFT}-1 \\ \text{IDFT}(S[k]H[k]) + \omega[n], & n = 0, \dots, N_{DFT}-1 \end{cases}, \tag{10}$$

where  $(*)$  represents the linear convolution,  $(\odot)$  denotes the circular convolution, and  $\text{IDFT}(\cdot)$  means IDFT operation.  $S[k]$  and  $H[k]$   $k = 0, \dots, N_{DFT}-1$  are the discrete Fourier transform (DFT) of time-domain transmitted signals and channel impulse response, respectively. Therefore, provided that  $N_{CP} \geq L$ , the linear and circular convolutions are equivalent for the receive samples at the indexes  $n = 0, \dots, N_{DFT}-1$ .

Furthermore, the circular convolution in time-domain means the multiplication in frequency-domain. It makes the frequency-domain equalizer (FDE) work in CE-OFDM fusion system. After CP samples are removed, FDE can be used to eliminate the channel distortion. Then, the following operations, which are inverse to those performed at the transmitter, are performed: a phase unwrap demodulator, followed by a DFT operation, then followed by a QAM demodulator.

For the simple AWGN case, the received signal is  $r[n] = s[n]e^{j\phi_0} + \omega[n]$ , where  $\phi_0$  is a phase offset of channel. The output of the phase demodulator is  $\hat{\phi}[n] = \phi[n] + \theta + \phi_0 + \xi[n]$ , where  $\xi[n] = \arctan\left[\frac{A_\omega[n] \sin[\phi_\omega[n] - \phi[n] - \theta - \phi_0]}{A + A_\omega[n] \sin[\phi_\omega[n] - \phi[n] - \theta - \phi_0]}\right]$  is the nonlinear noise component and the envelope and phase of AWGN is  $A_\omega[n] = |\omega[n]|$  and  $\phi_\omega[n] = \arctan[\omega[n]]$ .

The output of DFT following the phase demodulator is

$$Q[k] = \sum_{n=0}^{N_{DFT}-1} \hat{\phi}[n]e^{-j2\pi kn/N_{DFT}} = S[k] + \Phi[k] + N[k], \tag{11}$$

$k = 0, \dots, N_{DFT}-1$ . The signal component is

$$S[k] = \sum_{n=0}^{N_{DFT}-1} \phi[n]e^{-j2\pi kn/N_{DFT}} = 2\pi h C_{norm} \sum_{n=0}^{N_{DFT}-1} x[n]e^{-j2\pi kn/N_{DFT}}, \tag{12}$$

$$= 2\pi h \sqrt{2/(N\sigma_{PAM}^2)} X[k]$$

where  $C_{norm}$  is a constant, which is defined previously. The phase offset component is

$$\Phi[k] = \sum_{n=0}^{N_{DFT}-1} (\theta + \phi_0)e^{-j2\pi kn/N_{DFT}} = 0. \tag{13}$$

$k = 1, \dots, N_{DFT}-1$ . The noise component is

$$N[k] = \sum_{n=0}^{N_{DFT}-1} \xi[n]e^{-j2\pi kn/N_{DFT}}. \tag{14}$$

Assuming a high carrier-to-noise ratio (CNR),  $A \gg A_\omega[n]$ , and  $\xi[n]$  is well approximated as zero-mean Gaussian noise [17]. For the zero-mean Gaussian noise  $\xi[n]$ ,  $N[k]$  can also be approximated as zero-mean Gaussian random variable [17].

The output of DFT in receiver includes the signal component and AWGN in high CNR. The symbol error rate (SER) for the CE-OFDM system can be simplified to the problem of determining the SER for conventional PAM [29]. Therefore, the SER and BER are straightforward to express that [18]

$$SER \approx 2 \left( \frac{M-1}{M} \right) Q \left( 2\pi h \sqrt{\frac{6 \log_2 M \varepsilon_b}{M^2-1 N_0}} \right) \tag{15}$$

and

$$BER \approx \frac{SER}{\log_2 M} \approx 2 \left( \frac{M-1}{M \log_2 M} \right) Q \left( 2\pi h \sqrt{\frac{6 \log_2 M \varepsilon_b}{M^2-1 N_0}} \right), \tag{16}$$

where  $Q(x) = \int_x^\infty e^{-y^2/2} dy / \sqrt{2\pi}$  is the Gaussian  $Q$  function and  $\varepsilon_b = A^2 T / (2M \log_2 M)$  is the energy per bit of the CE-OFDM signal. The basic information demodulation and performance analysis of CE-OFDM communication is presented. For promoting RadCom performance, an additional multiple-access technique is required for multiple-user communication operation [30–32].

#### 4 CE-OFDM radar processing in frequency domain

The key issue of CE-OFDM radar system is that the implementation of wireless communication and environment sensing depends on same constant envelope

transmitted waveform. Meanwhile, the frequency-domain radar process is also an important part of CE-OFDM RadCom fusion approach. The radar process is based on the CE-OFDM signals which contain transmitted information of users. Therefore, the CE-OFDM fusion approach is able to complete communication and detection within the same spectrum simultaneously. This section will reveal an algorithm that allows for completing the radar detection only with the condition of the frequency-domain signal, instead of the baseband signals.

To make radar processing easier, the time-domain CE-OFDM multi-carrier transmitted signal can be expressed as [7–9].

$$x_{CE-OFDM}(t) = \sum_{\mu=0}^{N_{frame}-1} \sum_{n=0}^{N-1} S_{Tx}(\mu, n) \exp(j2\pi f_n t) \times \text{rect}[(t-\mu T_{OFDM})/T_{OFDM}] \quad (17)$$

where  $S_{Tx}(\mu, n)$  is the DFT of  $s[n]$  without oversampling.  $n$  represents the individual subcarrier index and  $\mu$  denotes the individual CE-OFDM symbol index.  $N_{frame}$  denotes the number of symbols.  $f_n$  is the individual subcarrier frequency,  $T_{OFDM} = T + T_{CP}$  is the total OFDM symbol duration, and  $\text{rect}(\cdot)$  describes a rectangular window of duration  $T_{OFDM}$ .

CE-OFDM RadCom signals are reflected by targets in the environment. Firstly, the CP of received signals is removed at the receiver. The time-domain signals without CP will be simultaneously sent to the communication processor and radar processor. The CE-OFDM received signal can also be expressed as the similar form

$$y_{CE-OFDM}(t) = \sum_{\mu=0}^{N_{frame}-1} \sum_{n=0}^{N-1} S_{Rx}(\mu, n) \exp(j2\pi f_n t) \times \text{rect}[(t-\mu T_{OFDM})/T_{OFDM}] \quad (18)$$

where  $S_{Rx}(\mu, n)$  is the DFT of the received signals without CP.

With the orthogonality between individual subcarriers, the following relation must hold [8]:

$$f_n = n \times \Delta f = n/T, \quad n = 0, \dots, N-1, \quad (19)$$

where  $\Delta f$  expresses the orthogonality between subcarriers, which is the reciprocal of the elementary OFDM symbol duration.

For the ground transportation application, it is expected that the received signal is shifted in frequency due to a relative velocity between the radar platform and reflecting objects. In the case of the radar application

between radar and target moving with relative velocity  $v_{rel}$ , the Doppler frequency shift  $f_D$  at the receiver is [1]

$$f_D = 2v_{rel}/\lambda = 2v_{rel}f_c/c, \quad (20)$$

where  $\lambda$  is the wavelength,  $f_c$  is the carrier frequency, and  $c$  is speed of light.

If a CE-OFDM signal is reflected at an object in the range  $R$  with a Doppler shift  $f_D$  due to a relative movement between the transmitter and the reflecting object, the received signal can be expressed as

$$y_{CE-OFDM}(t) = \sum_{\mu=0}^{N_{frame}-1} \sum_{n=0}^{N-1} A(\mu, n) S_{Tx}(\mu, n) \times \exp\left[j2\pi f_n \left(t - \frac{2R}{c}\right)\right] \exp(j2\pi f_D t), \quad (21)$$

$$\times \text{rect}\left[\left(t - \mu T_{OFDM} - \frac{2R}{c}\right)/T_{OFDM}\right]$$

with  $A(\mu, n)$  being the signal amplitude. In order to make the different influence between Doppler and range more obvious, the received signal can be rearranged into

$$y_{CE-OFDM}(t) = \sum_{\mu=0}^{N_{frame}-1} \exp(j2\pi f_D t) \sum_{n=0}^{N-1} A(\mu, n) \times S_{Tx}(\mu, n) \exp\left(-j2\pi f_n \frac{2R}{c}\right) \exp(j2\pi f_n t) \times \text{rect}\left[\left(t - \mu T_{OFDM} - \frac{2R}{c}\right)/T_{OFDM}\right] \quad (22)$$

The receiver observes the received signal only in the elementary OFDM symbol duration to recover one CE-OFDM symbol. When the appropriate CP duration has been chosen, the receiver will still cut the observed samples from the same CE-OFDM symbol. Therefore, the time shift of the rect-function in the above two formulas can be omitted. When the CE-OFDM signal bandwidth is much smaller than the carrier frequency, Doppler frequency results in a uniform phase shift on every subcarrier [1]. Besides, for a fixed subcarrier index  $n$ , the Doppler effect introduces a linear phase shift,  $2\pi f_D T_{OFDM}$ , between the consecutive frequency symbols. Furthermore, the phase change of the range is the same on one subcarrier in one frame time. When  $A(\mu, n)$  is constant and ignored, the received signals can also be rewritten as:

$$y_{CE-OFDM}(t) = \sum_{\mu=0}^{N_{frame}-1} \sum_{n=0}^{N-1} S_{Tx}(\mu, n) \exp(j2\pi \mu f_D T_{OFDM}) \times \exp\left(-j2\pi f_n \frac{2R}{c}\right) \exp(j2\pi f_n t) \quad (23)$$

And it is clear that the received frequency-domain symbols can be quantified as

$$\begin{aligned}
 S_{Rx}(\mu, n) &= S_{Tx}(\mu, n) \exp\left(-j2\pi f_n \frac{2R}{c}\right) \\
 &\quad \times \exp(j2\pi\mu f_D T_{OFDM}) \\
 &= S_{Tx}(\mu, n) \exp\left(-j2\pi n \Delta f \frac{2R}{c}\right) \cdot \\
 &\quad \times \exp\left(j2\pi\mu T_{OFDM} \frac{2v_{rel} f_c}{c}\right)
 \end{aligned} \tag{24}$$

It is clear that, the influence of range and the Doppler frequency from relative velocity is completely orthogonal in frequency domain. While the Doppler introduces a linear phase shift only along the time axle, the range also introduces a linear phase shift along the frequency axle. If the observation duration is short enough, the reflecting object remains within one range resolution cell. As a result, this orthogonality can be satisfied. Therefore, it must search for a suitable processing algorithm to recover range and Doppler independently.

In order to make the target detection process arrive at a more descriptive representation, a matrix is applied to denote the frequency-domain symbol frame in (25). In the matrix, every row represents a vector composed of time-domain samples in one subcarrier, whereas each column represents one CE-OFDM symbol consisting of different subcarrier samples. That is, vertical axle is the frequency axle and abscissa axle is the time axle, which makes the frequency-domain symbols arranged in time-frequency space. This rearrangement can be used to represent both the transmitted and the received frequency-domain symbols.

$$\mathbf{D} = \begin{pmatrix} S(0,0) & S(1,0) & \cdots & S(N_{frame}-1,0) \\ S(0,1) & S(1,1) & \cdots & S(N_{frame}-1,1) \\ \vdots & \vdots & \ddots & \vdots \\ S(0,N-1) & S(1,N-1) & \cdots & S(N_{frame}-1,N-1) \end{pmatrix} \tag{25}$$

It makes the row vector

$$\vec{k}_R = [0, \exp(-j2\pi\Delta f 2R/c), \dots, \exp(-j2\pi(N_c-1)\Delta f 2R/c)] \tag{26}$$

and another row vector

$$\vec{k}_D = [0, \exp(j2\pi T_{OFDM} 2v_{rel} f_c/c), \dots, \exp(j2\pi(N_{frame}-1) T_{OFDM} 2v_{rel} f_c/c)] \tag{27}$$

where  $k_R(n) = \exp(-j2\pi n \Delta f 2R/c)$ ,  $n = 0, \dots, N-1$ , and  $k_D(\mu) = \exp(j2\pi\mu T_{OFDM} 2v_{rel} f_c/c)$ ,  $\mu = 0, \dots, N_{frame}-1$ . The vector  $\vec{k}_R$  and the vector  $\vec{k}_D$  describe the influence of range and the Doppler introduced by the reflecting object on the received frequency-domain symbols.

To obtain the range and relative velocity of the reflecting object, it first achieves an element-wise multiplication between the transmitted and received frequency-domain symbol matrices. With the same matrix

representation, the quotient matrix of the frequency-domain symbols is provided

$$(\mathbf{D}_{div})_{\mu,n} = (\mathbf{D}_{Rx})_{\mu,n} / (\mathbf{D}_{Tx})_{\mu,n} = \vec{k}_R^T \cdot \vec{k}_D \tag{28}$$

with  $(\cdot)^T$  being the matrix transpose operation and  $(\cdot)$  being the matrix multiplication operation. It shows clearly that influence of range and the Doppler of the reflecting object is orthogonal. To observe the relation of range and Doppler in element level, the above equation can be rewritten in terms of the range factor  $k_R(n)$  and the Doppler factor  $k_D(\mu)$  as

$$\begin{aligned}
 \frac{S_{Rx}(\mu, n)}{S_{Tx}(\mu, n)} &= k_R(n) \times k_D(\mu) \\
 &= \exp\left(-j2\pi n \Delta f \frac{2R}{c}\right) \exp\left(j2\pi\mu T_{OFDM} \frac{2v_{rel} f_c}{c}\right).
 \end{aligned} \tag{29}$$

In one CE-OFDM symbol, the range  $R$  is translated into a linear phase shift between subcarriers on one frequency-domain symbol. Computing the IDFT of  $k_R(n)$  is the most convenient way to obtain the range to the target

$$\begin{aligned}
 r(p) &= \text{IDFT}(k_R(n)) = \frac{1}{N} \sum_{n=0}^{N-1} k_R(n) \exp\left(j2\pi \frac{n}{N} p\right) \\
 &= \frac{1}{N} \sum_{n=0}^{N-1} \exp\left(-j2\pi n \Delta f \frac{2R}{c}\right) \exp\left(j2\pi \frac{n}{N} p\right),
 \end{aligned} \tag{30}$$

with  $p = 0, \dots, N-1$ . It can be seen that, the two exponential terms in the above equation cancel each other out and result in unity, under the condition

$$p = \left\lfloor \frac{2R\Delta f N}{c} \right\rfloor, \quad p = 0, \dots, N-1 \tag{31}$$

where  $\lfloor \cdot \rfloor$  represents round-down operation. This means that a peak will occur at this index of  $p$  in the IDFT result within a target in the environment.

In a similar way, the relative velocity  $v_{rel}$  is translated into a linear phase shift between the frequency-domain symbols on the time axle. The relative velocity  $v_{rel}$  can be easily solved by applying a DFT

$$\begin{aligned}
 v(l) &= \text{DFT}(k_D(\mu)) = \sum_{\mu=0}^{N_{frame}-1} k_D(\mu) \exp\left(-j2\pi \frac{\mu}{N_{frame}} l\right) \\
 &= \sum_{\mu=0}^{N_{frame}-1} \exp\left(j2\pi\mu T_{OFDM} \frac{2v_{rel} f_c}{c}\right) \exp\left(-j2\pi \frac{\mu}{N_{frame}} l\right)
 \end{aligned} \tag{32}$$

with  $l = 0, \dots, N_{frame}-1$ . When the condition has been satisfied,

$$l = \left\lfloor \frac{2v_{rel}f_c T_{OFDM}N_{frame}}{c} \right\rfloor, \quad l = 0, \dots, N_{frame}-1 \quad (33)$$

It can be seen that the two exponential terms in the above equation cancel each other out, and a peak will occur at this index of  $l$  in the DFT result within a target in environment. Hence, the array process for range is to compute the IDFT of  $\mathbf{D}_{div}$  along the time axle. And then, along the spectrum axle, the DFT of the gotten matrix is a result of the array process.

The processing methods of range and relative velocity are completely independent from the transmitted information. The typical Fourier side lobes ensure a high dynamic range performance. All processing operations are linear, and it guarantees that this processing approach will operate for an unlimited number of targets with different ranges and Doppler frequency.

In summary, the received frequency-domain symbol matrix  $\mathbf{D}_{Rx}$  is indispensable for the detection processing algorithm and the key of the algorithm is the previous element-wise complex division. At last, the matrix result is a two-dimensional radar image in range and relative velocity.

On account of the unique radar processing, peak value in the radar image cannot represent the processing gain of CE-OFDM RadCom system. Specifically, the RadCom signals obtain a total power gain of  $N^2$  after a Fourier transform, which is a coherent deterministic process. However, after a Fourier transform, only a power gain of  $N$  is added for the noise, which is a random quantity. Therefore, for CE-OFDM RadCom fusion system, the radar processing gain is expressed as

$$G_p = NN_{frame}. \quad (34)$$

The radar function of CEOFDM RadCom fusion system is based on radar processing in frequency domain. And the main frequency domain processing lies on the computation of DFT, which is a standard procedure that can be efficiently implemented at present.

### 5 Simulation and analysis methods

The simulation of this article is based on the Matlab software and the Windows 7 desktop system. The parameters in Table 1 are satisfied. Following the structure of CE-OFDM RadCom fusion system, the BER simulation results with turbo code (code length = 1008 and code rate = 1/3) have been obtained in AWGN channel and multipath channel. The ambiguity function simulation and multiple target detection of the CE-OFDM RadCom system are also completed.

The Neyman-Pearson criterion states that  $P_d$  is the biggest detection probability when a specific false alarm probability is satisfied with a given SNR. According to

this criterion, the output maximum of the array processor is measured to obtain the detection threshold of 0.001 false alarm probability, when only 0 dB SNR AWGN is received. Since the special radar process algorithm requires the known transmitted signals, the detection threshold with different symbol modulation order and modulation index is simulated in Fig. 11. With the fixed false alarm probability, the detection threshold with any SNR is linearly correlated with the detection threshold with 0 dB SNR. The detection probability, with different detection threshold data in Fig. 11, is simulated within different SNR in Fig. 12 to verify the effectiveness of obtained detection threshold.

### 6 Simulation and analysis results for communication

The RadCom fusion system is able to exchange real-time mutual information and remove the external interference between wireless communication and radar systems. Specifically for the road safety, the CE-OFDM RadCom system contributes the cars in not only information sharing, but also completing the range and relative velocity information detecting by other cars. Normally, the industrial, scientific, and medical (ISM) bands can be used for any device without requiring a license. The radar application requires at least 100 MHz bandwidth for sufficient detection resolution. The 24-GHz ISM band is the lowest worldwide available ISM band that satisfies this requirement [1]. However, the achievable range for communications decreases with increasing carrier frequency due to the influence of free space attenuation and diffraction. Therefore, in this paper, the 24-GHz ISM band is considered as a suitable frequency band for integrated RadCom fusion systems. In Table 1, a complete set of OFDM system parameters

**Table 1** CE-OFDM system parameters for vehicle network

Symbol	Parameter	Value
$f_c$	Carrier frequency	24 GHz
$N$	Number of subcarrier	1024
$J$	Oversampling factor	8
$\Delta f$	Subcarrier spacing	90.909 kHz
$T$	Elementary OFDM symbol duration	11 $\mu$ s
$T_{CP}$	Cyclic prefix length	1.375 $\mu$ s
$T_{OFDM}$	Total OFDM symbol duration	12.375 $\mu$ s
$B$	Signal bandwidth	93.1 MHz
$\Delta R$	Radar range resolution	1.61 m
$R_{max}$	Maximum detection range	1650 m
$\Delta v$	Radar velocity resolution	1.97 m/s
$v_{max}$	Maximum detection velocity	252.3 m/s
$N_{frame}$	Number of evaluated symbols	256

is provided, which satisfies general conditions for vehicles. The maximum absolute value of the Doppler shift  $f_D$  is limited by the OFDM symbol duration. The maximum absolute Doppler shift can be measured as  $1/(2T_{OFDM})$ . Notice that, in this paper, performances of wireless communication and radar detection are separately discussed in two different sections. In this section, performances of wireless communications are presented.

Figure 5 presents the BER performance of CE-OFDM with the rise of the energy per bit to noise power spectral density ratio ( $E_b/N_0$ ) in the presence of AWGN channels. According to [18], phase offset (PO) is a key factor for phase modulated signals. When  $M_{QAM} = 4$ , Fig. 5 presents BER performance of CE-OFDM RadCom with and without PO in AWGN channel. The turbo code (code length =1008 and code rate =1/3) is applied for improving BER performance.

It is clear that BER performance becomes worse when choosing a lower modulation index, i.e.,  $2\pi h = 0.5$ . With  $2\pi h = 1$ , the best BER performance with turbo encoding is achieved, which is about 0.00001 with 4 dB  $E_b/N_0$ . The BER performance curves with and without PO almost coincide. It proves that the phase unwrap demodulator can remove the phase offset in channel.

Since the inherent property of CE-OFDM,  $2\pi h = 1$  means real value OFDM time-domain signals mapping into the phase space. When  $2\pi h$  is bigger than 1, CE-OFDM system performance also degenerates, because some phase value is over  $(-\pi, \pi)$ , which cannot be recovered. As a result, these simulation results prove that the phase unwrap receiver could remove the phase offset and recover phase information.

In this paper, frequency-domain equalization is simplified with the conventional transmission used in OFDM

systems. The circular convolution in time-domain leads to the vector multiplication in frequency-domain. Therefore, the channel distortion can be dispensed in a simple way. The frequency-domain minimum mean-squared error (MMSE) equalizer definition is [33].

$$C[k] = \frac{H^*[k]}{|H[k]|^2 + (\epsilon_b/N_0)^{-1}}, k = 0, \dots, N_{DFT}-1 \quad (35)$$

where  $(\cdot)^*$  represents the conjugate operation. The output of the equalizer can be simplified as  $\hat{s}[n] = \text{IDFT}\{R[k]C[k]\}$ ,  $n = 0, \dots, N_{DFT} - 1$ .

With the turbo encoding (code length =1008 and code rate =1/3) and  $M_{QAM} = 4$ , Fig. 6 shows the CE-OFDM BER performance with MMSE equalizer in the presence of multipath fading channels with different numbers of multipath, such as 5 paths, 10 paths, and 64 paths. The CE-OFDM BER performance with 5 paths about 1 dB is worse than that with 10 paths OFDM at 12 dB  $E_b/N_0$ . Compared with 64 paths, channel response with 5 or 10 paths has greater influence on CE-OFDM BER performance. When the number of channel multipath is 64, the CE-OFDM BER performance is almost the same as 5 or 10 paths CE-OFDM BER at  $E_b/N_0 = 5$  dB and then it declines rapidly. When  $E_b/N_0$  is 13 dB, the CE-OFDM BER with 64 paths is around 0.0001. It proves that the BER performance of CE-OFDM RadCom systems is improved with the increasing number of path, which means it is able to achieve multipath diversity. As the input of the phase modulator is real-valued OFDM signals, every CE-OFDM symbol data is extended into the multipath frequency point. Hence, CE-OFDM RadCom system exploits multipath gain.

The fact that CE-OFDM exploits multipath diversity is interesting since traditional OFDM does not [34]. The diversity gain in CE-OFDM is explained by viewing the Taylor series expansion of the CE-OFDM transmitted signal

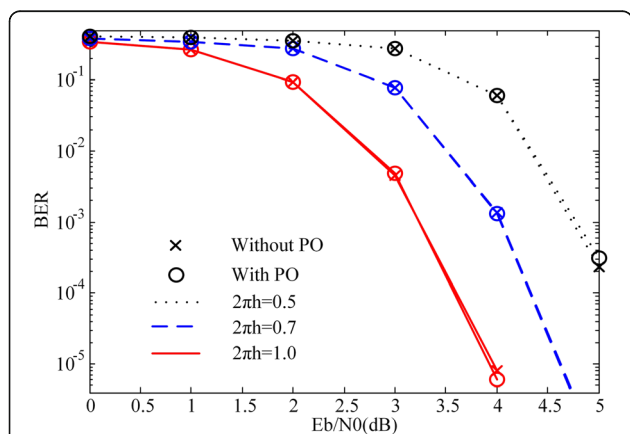


**Fig. 5** BER performance of CE-OFDM with and without phase offset. Detailed legend: the cross represents simulation without phase offset and the circle represents simulation with phase offset. The dotted line, the broken line, and the full line represents  $2\pi h = 0.5, 0.7$ , and  $1.0$ , respectively

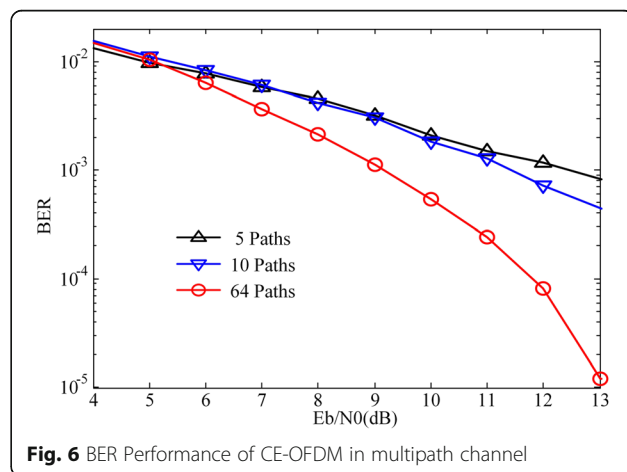


**Fig. 6** BER Performance of CE-OFDM in multipath channel

$$s(t) = Ae^{j\phi(t)} = A \left[ 1 + j\phi(t) - \frac{\phi^2(t)}{2!} - j\frac{\phi^3(t)}{3!} + \dots \right] \quad (36)$$

The higher-order terms of  $\phi(t)$  lead to an  $n$ -fold frequency-domain convolution and the frequency-domain spreading of the data symbols. Therefore, the promotion of performance in multipath channels results from the frequency-domain spreading.

## 7 Simulation and analysis results for detection

### 7.1 The ambiguity function graph

The ambiguity function is defined as [22]

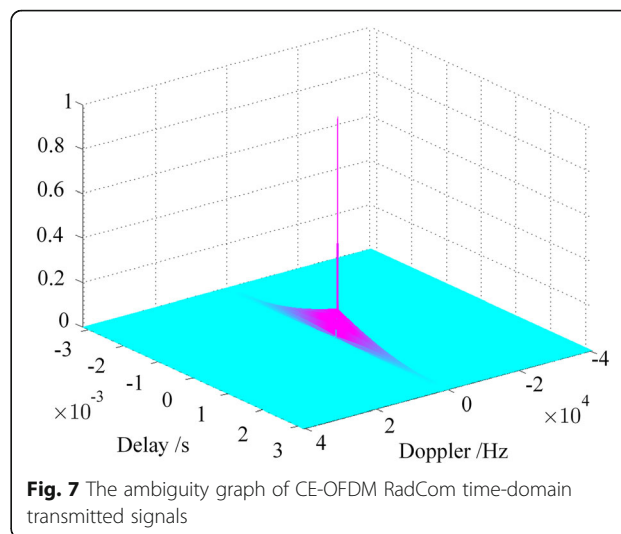
$$|\chi(\tau, f_d)|^2 = \left| \int_{-\infty}^{\infty} s(t)s^*(t-\tau)e^{j2\pi f_d t} dt \right|^2. \quad (37)$$

The three-dimension graph, which is obtained by  $|\chi(\tau, f_d)|^2$ , is called the ambiguity graph. Meanwhile, the ambiguity graph displays the delay ambiguity and Doppler ambiguity caused by the neighbor target with a single peak lying in the center of the ambiguity graph. In engineering application, the sectional view of given height, like  $-3$  dB, is often used to denote the ambiguity graph.

The ambiguity function of radar signals should be focused on a single peak, and other energy is distributed on delay-Doppler plane averagely. The radar ambiguity function is always used as a tool to investigate different waveforms and to determine the range resolution and the Doppler resolution of the special waveform. Ambiguity function can estimate parameters about accuracy and resolution of range and relative velocity of single target. Multiple targets can be distinguished according to these parameters.

For wireless communication systems, ambiguity function is defined the same as the radar ambiguity function. For avoiding ISI and ICI, it requires signals to satisfy orthogonality, and the shaping pulse function needs the characteristic of time-frequency localization. Therefore, wireless communication ambiguity function are often used to observe the orthogonality and the time-frequency localization property of signals.

Assuming that various wireless signals are utilized in detection procedure, the detection performance value can be derived from its ambiguity graph. With the parameters in Table 1 being fulfilled, Fig. 7 represents the simulation result from a server and the MATLAB software, in which the  $1152 \times 256 = 294,912$  length CE-OFDM RadCom time-domain transmitted signals are calculated by ambiguity function. Figure 7 demonstrates that there is only one peak in the center of the ambiguity graph of CE-OFDM RadCom transmitted signals. The range resolution and the Doppler resolution are small enough. This proves the CE-OFDM RadCom signal fits common requirements of radar detection.



### 7.2 Detection in multiple target scenario

The process methods of range and relative velocity for CE-OFDM RadCom system are completely independent from the transmitted information. Furthermore, all processing operations are linear, and it can operate for an unlimited number of targets with different ranges and Doppler frequency. In this section, three targets with different ranges and Doppler frequency are assumed in environment.

Table 2 defines three targets in environment with different range and relative velocity information: target 1 and target 2 with the same range and target 2 and target 3 with the same relative velocity. Figure 8 presents the radar display graph of detection with the three targets.

In 24-GHz ISM band, with the parameters in Table 1 being fulfilled, the radar detection is simulated in Fig. 8 when signal-to-noise ratio (SNR) is 1 dB. Three peaks that represent three targets can be explicitly found in the graph.

With three rhombus points, the  $-6$ -dB sectional view, in which the central coordinate point means the information of relative velocity and range, is demonstrated in Fig. 9. Three points can be acquired from the view. The estimated values in the figure are almost the same as the target parameters. This proves that the targets with the same range or relative velocity can be separated by the frequency-domain process. Hence, the frequency-domain radar process is able to operate for multiple target scenarios within appropriate resolution.

**Table 2** Range and relative velocity parameters for three targets

Target	Range/m	Relative velocity/m/s
1	500	-200
2	500	-150
3	400	-150

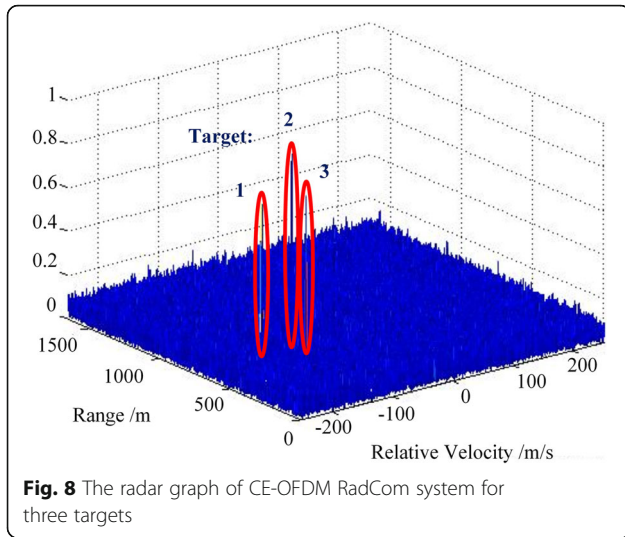


**Fig. 8** The radar graph of CE-OFDM RadCom system for three targets

In dynamic range, the reflecting targets are denoted as peaks in radar display graph, which means fine detection performance of the CE-OFDM RadCom system. The simulation environment is multipath fading channel with 1 dB SNR, and the side-lobe peak value is 0.1, which is not able to affect target detection due to the unique process property of CE-OFDM RadCom system. Furthermore, the radar processing approach can achieve the target information without amplifying noise.

### 7.3 Detection threshold

Radar detection is a very complex process. When there is a target in environment, the probability that the target is successfully detected by the radar system is defined as the detection probability [35],  $P_d$ . When there is no target in environment, the probability of false alarm for radar is the false alarm probability,  $P_{fa}$ . The detection probability is an important parameter for radar systems.

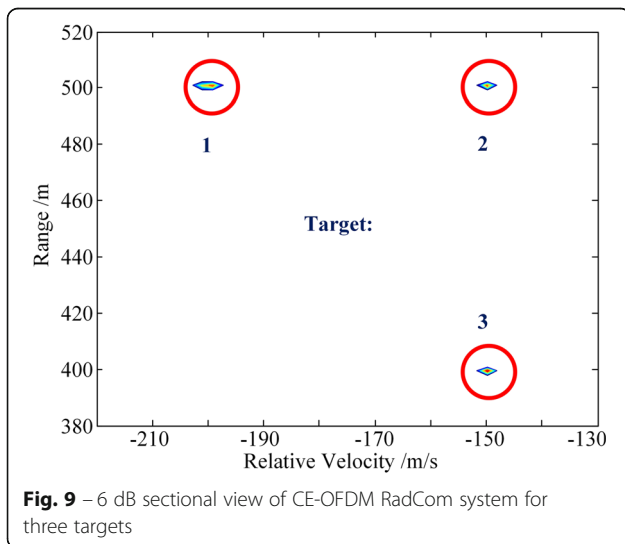


**Fig. 9** -6 dB sectional view of CE-OFDM RadCom system for three targets

However, the detection probability is not fixed. In a real detection system, the detection probability depends on a detection threshold, which lies on the requirements for false alarm probability and SNR.

The Neyman-Pearson criterion is widely applied in radar signal detection. This criterion states that  $P_d$  is the biggest detection probability when a specific false alarm probability is satisfied with a given SNR [35]. Therefore, the confirmation of detection probability for a radar system is complicated. The detection threshold is the basis of achieving detection probability. Following the Neyman-Pearson criterion, the detection threshold depends on one specific false alarm probability with a given SNR. The signals of common radar system are definite while the signals of CE-OFDM RadCom system are random for the signal phase.

Figure 10 shows structure of the frequency-domain detection processor in the CE-OFDM RadCom fusion system. In this detection algorithm, the reference signal is the CE-OFDM transmitted signal  $s(t)$ , which contains user random data in its phase. Reference signals and received signals are mapped into frequency symbols by DFT. After the element-wise division, the matrix will be passed an array processor, including range and velocity extraction. And the gotten matrix result could form the three-dimension radar image. Then, the target detector will make a decision according to the detection threshold. If one peak is bigger than the detection threshold, the target detector outputs the range and velocity information about the peak, which means one target has been detected.

Since the user random data is transmitted, the reference signal varies with different data and modulation in the CE-OFDM RadCom fusion system. For the unique radar process in frequency domain, the user data has no influence on detection. However, detection threshold is obtained when only AWGN is received. And the array processing is a linear procedure, so it has no effect on the detection threshold confirmation. In another word, the detection threshold only depends on reference signals with a specific  $P_{fa}$  and a given SNR. The given SNR is denoted as  $\alpha = E_s/N_0$ , where  $E_s$  is symbol energy and  $N_0$  is power spectral density (PSD) of AWGN. When input of detection receiver is AWGN, the output matrix of array processor can be expressed as

$$\begin{aligned} \mathbf{r}_\alpha &= \text{IDFT}(\text{DFT}(\mathbf{D}_{div})) = \text{IDFT}\left(\text{DFT}\left(\frac{\Omega_\alpha}{\mathbf{S}_{Tx}}\right)\right), \\ &= \text{IDFT}\left(\text{DFT}\left(\frac{\text{DFT}(\omega_\alpha)}{\mathbf{S}_{Tx}}\right)\right) \end{aligned} \tag{38}$$

where  $\mathbf{D}_{div}$ ,  $\Omega_\alpha$ , and  $\mathbf{S}_{Tx}$  are the result matrix of elementary division, DFT of AWGN, and DFT of reference

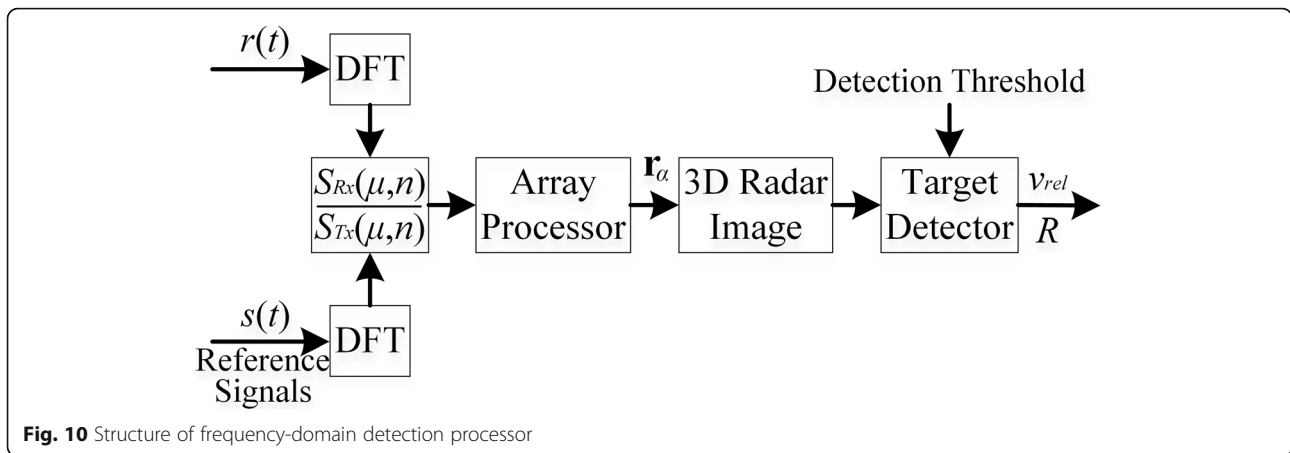


Fig. 10 Structure of frequency-domain detection processor

signals, respectively.  $\omega_\alpha$  is the AWGN matrix.  $IDFT(\cdot)$  and  $DFT(\cdot)$  are IDFT operation and DFT operation. The output value of array processor is  $r \in \mathbf{r}_\alpha$ ; the cumulative distribution function (CDF) of  $r$  can be expressed as

$$F_r(x) = P(r \leq x) = \int_{-\infty}^x f_r(t) dt, \quad (39)$$

where  $f_r(t)$  is probability density function (PDF) of  $r$ . The CDF of  $r$  is the probability that  $r$  is lower than the fixed value  $x$ . When the detection threshold is defined as  $D_{T,\alpha}$ , the false alarm probability can be represented as

$$P_{fa,\alpha} = \int_{D_{T,\alpha}}^{+\infty} f_r(t) dt = 1 - F_r(D_{T,\alpha}). \quad (40)$$

The detection threshold of a given false alarm probability can be obtained in the CDF results of output value of array processor. When received signals are AWGN, the output of elementary division can be expressed as

$$\mathbf{D}_{div} = \frac{\Omega_\alpha}{\mathbf{S}_{Tx}} = \frac{DFT(\omega_\alpha)}{DFT\left(\left(\exp(j2\pi h C_{norm} x[i])\right)_{i=0}^{N-1}\right)}. \quad (41)$$

For the CE-OFDM fusion system, the denominator of the equation defines the DFT of CE-OFDM reference signal, which varies with modulation index  $h$ , normalization constant  $C_{norm}$ , and real-valued OFDM signal  $x[i]$ . Since user random data is necessary,  $C_{norm}$  and  $x[i]$  depend on the symbol modulation order  $M_{QAM}$ . As a consequence,  $\mathbf{D}_{div}$  relates with modulation index  $h$ , symbol modulation order  $M_{QAM}$ .

In the frequency-domain detection algorithm, the output of array processor is influenced by user random data. The detection threshold not only depends on the false alarm probability  $P_{fa}$  and SNR, but also depends on the symbol modulation order  $M_{QAM}$  and phase modulation index  $h$ . Although the confirmation of detection

threshold is complicated, detection threshold is a necessity for detection probability, which is an important radar parameter. With a given false alarm probability and SNR, the detection threshold  $D_{T,\alpha}$  can be obtained by simulating the CDFs of output value of array processor for CE-OFDM fusion approach. Especially the modulation of 4QAM is the same as quadrature phase shift keying (QPSK). Therefore, QPSK represents the modulation with  $M_{QAM} = 4$ .

Provided that the false alarm probability is 0.001 and SNR is 0 dB, the input of detection receiver is only AWGN and the parameters in Table 1 have been fulfilled. Figure 11 displays the simulation result about the detection threshold with a different symbol modulation order  $M_{QAM}$  and modulation index  $h$  for CE-OFDM RadCom fusion systems. Since all envelopes of reference signals are constant and the detection process is

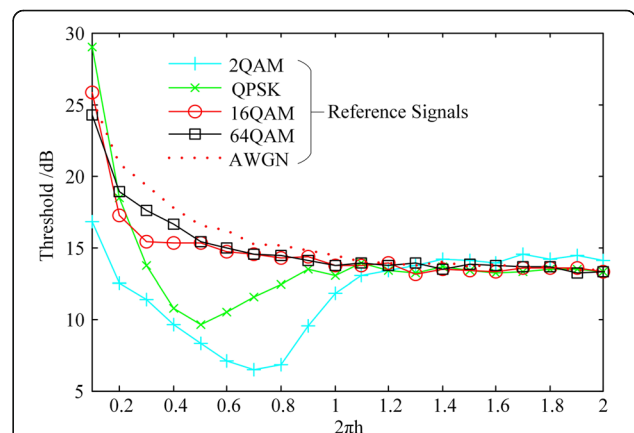


Fig. 11 The detection threshold of CE-OFDM RadCom system for different MQAM and  $2\pi h$ . Detailed legend: the lines with the plus sign, cross, circle, and square represent 2QAM, QPSK, 16QAM, and 64QAM being used to produce reference signals, respectively. The dotted line represents the AWGN used for producing reference signals. In Fig. 11, the threshold value means the setting threshold for 0.001 false alarm probability and 0 dB SNR

complex, the detection processing result is not normalized. Therefore, when the detection threshold is smaller, the detection probability will be higher with a given SNR and a given false alarm probability.

These five curves represent the threshold results of different reference signals in Fig. 11, which are generated from the transmitter with different input symbols. The modulation index  $h$  is a parameter, which relates with the stochastic distribution of phase of constant envelope signals in  $(-\pi, \pi]$ . When the phase modulation index is big enough,  $2\pi h \geq 1.2$ , the phase distribution of reference signals is almost random and the curves trend to be flat and the detection threshold trends to be a constant, about 13.8 dB. When modulation order is big,  $M_{QAM} = 16$  or 64, and phase modulation index is small,  $2\pi h < 0.3$ , the phase value of reference signals is very small, which results in the high detection threshold.

It is unexpected that the threshold curves of QPSK reference signals and 2QAM reference signals at first declines with  $2\pi h$  and then rises to about 14 dB. The smallest threshold value of QPSK reference signals is about 10 dB with  $2\pi h = 0.5$ , and the smallest threshold value of 2QAM is around 7 dB with  $2\pi h = 0.7$ . The low modulation order,  $M_{QAM} = 2$  or 4, and appropriate phase modulation index,  $0.3 < 2\pi h < 0.9$ , result that the phase distribution of reference signals is more nonrandom. And the nonrandom phase distribution affects the variance of  $1/S_{Tx}$ , which is a part of  $\mathbf{D}_{div}$ . As a result, symbol modulation order  $M_{QAM}$  and modulation index  $h$  are important parameters for the detection threshold of the CE-OFDM RadCom fusion system.

#### 7.4 Detection probability

When input of detection receiver is AWGN with a given  $\alpha$ , provided that  $M_{QAM}$  and  $2\pi h$  are fixed, the output matrix of array processor can be expressed as

$$\begin{aligned} \mathbf{r}_\alpha &= \text{IDFT} \left( \text{DFT} \left( \frac{\text{DFT}(\boldsymbol{\omega}_\alpha)}{\mathbf{S}_{Tx}} \right) \right) = \text{IDFT} \left( \text{DFT} \left( \frac{\text{DFT}(c\boldsymbol{\omega}_{\alpha=1})}{\mathbf{S}_{Tx}} \right) \right) \\ &= c \cdot \text{IDFT} \left( \text{DFT} \left( \frac{\text{DFT}(\boldsymbol{\omega}_{\alpha=1})}{\mathbf{S}_{Tx}} \right) \right) = c \cdot \mathbf{r}_{\alpha=1}, \end{aligned} \tag{42}$$

where  $c$  is proportion coefficient of input noise amplitude and  $\boldsymbol{\omega}_\alpha = c\boldsymbol{\omega}_{\alpha=1}$ . Since IDFT operation and DFT operation are both linear operations, the change of  $\alpha$  leads to the linear change of  $\mathbf{r}_\alpha$ . With 0 dB SNR,  $\alpha = 1$  and  $N_{0, \alpha=1}$  is the PSD of AWGN. Since  $\alpha = E_s/(c^2 N_{0, \alpha=1}) = 1/c^2$ , it is visible that  $D_{T,\alpha} = cD_{T,1} = D_{T,1}/\sqrt{\alpha}$ , where  $D_{T,1}$  can be obtained according to Fig. 11. It is clearly visible that the detection threshold with 0 dB SNR has a linear correlation with the threshold with other SNR. When the input of detection processor is the reflected CE-OFDM signal and AWGN, detection probability for the CE-OFDM RadCom

system is defined as the probability that the maximum output value of detection processor is higher than  $D_{T,\alpha}$ . Therefore, detection probability for the CE-OFDM RadCom system could be expressed according to  $D_{T,\alpha}$  and the PDF of  $r \in \mathbf{r}_\alpha$ :

$$P_d(\alpha) = \int_{D_{T,\alpha}}^{+\infty} f_r(t)dt = \int_{D_{T,1}/\sqrt{\alpha}}^{+\infty} f_r(t)dt. \tag{43}$$

With  $P_{fa} = 0.001$  and the detection threshold  $D_{T,1}$  in Fig. 11, the Fig. 12 represents the detection probability of the CE-OFDM RadCom system for a different symbol modulation order  $M_{QAM}$  and different modulation index  $h$ . The detection probability curves rise with the increasing SNR for CE-OFDM RadCom system. When 99% detection probability is obtained, the smaller required SNR is better. When  $2\pi h = 0.3$ , required SNR of 99% detection probability rises with  $M_{QAM}$ . When  $2\pi h = 0.7$  or 1.0, required SNR of 99% detection probability is smallest with 2QAM and the required SNR with 16/64QAM are almost the same and biggest. When  $2\pi h = 1.4$ , required SNR of 99% detection probability rises with QPSK/16QAM/64QAM are nearly the same, but the required SNR with 2QAM is biggest.

With a different modulation index and different symbol modulation order, the results of detection probability for CE-OFDM RadCom system confirm the validity of corresponding detection threshold of  $P_{fa} = 0.001$  and 0 dB SNR in Fig. 11. The smallest required SNR of 99% detection probability, -17 dB, is obtained under the condition 2QAM and  $2\pi h = 0.7$ .

The CE-OFDM RadCom system exploits CE-OFDM signals with user information to complete environment sensing. The achievement of detection probability in this system is more complex than traditional radar system. The variation of reference signals must be taken into consideration, and it is significant to investigate RadCom system with a single waveform.

#### 8 Conclusions

A joint radar and wireless communication fusion system is the technology development tendency of future intelligence wireless system. Focusing on high PAPR problem of traditional broadband multicarrier waveform, a new CE-OFDM RadCom fusion approach is introduced in this paper. This RadCom fusion system is composed of CE-OFDM wireless communication system and the frequency-domain radar processing. The PAPR of CE-OFDM RadCom signals is constant 0 dB. The high PAPR problem of traditional broadband multicarrier waveform is solved effectively. The constant envelope process and information demodulation are described and analyzed. And the frequency-domain radar processing is introduced. Then, the CE-OFDM RadCom fusion

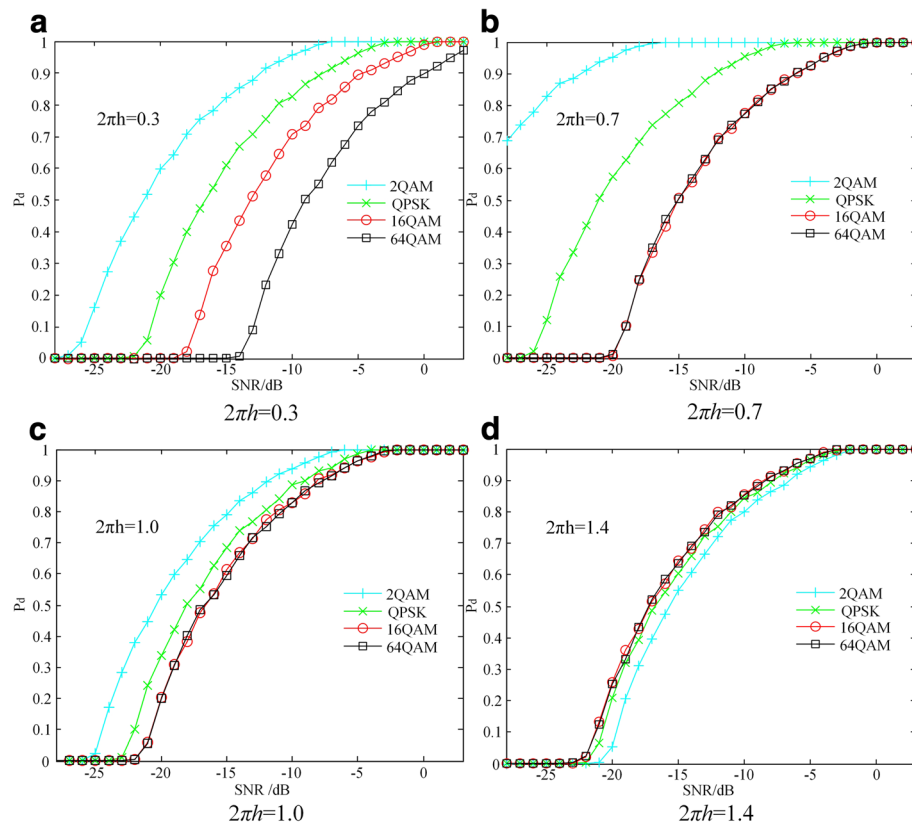


**Fig. 12** The detection probability of CE-OFDM RadCom system for different MQAM and  $2\pi h$ . Detailed legend: with 0.001 false alarm probability, the threshold data in Fig. 11 is used to simulate the detection probability for the CE-OFDM RadCom system. The lines with the plus sign, cross, circle, and square represent 2QAM, QPSK, 16QAM, and 64QAM being used to produce the CE-OFDM RadCom signals, respectively. The  $2\pi h$  is different. **a**  $2\pi h = 0.3$ , **b**  $2\pi h = 0.7$ , **c**  $2\pi h = 1.0$ , **d**  $2\pi h = 1.4$

system is simulated with a series of parameters in a 24-GHz ISM band. Simulation results demonstrate that CE-OFDM RadCom system is able to communicate with high data rate and exploit multipath gain in multipath channel. Meanwhile, the ambiguity image of transmitted CE-OFDM RadCom signals is achieved with the high resolution for detection. Finally, the detection threshold and the detection probability of CE-OFDM RadCom fusion system is simulated and analyzed according to the Neyman-Pearson criterion. The further work will focus on enhancing the array detection algorithm and improving the RadCom technique for satellite traffic recognition and telemetry.

**Abbreviations**

AWGN: Additive white Gaussian noise; BER: Bit error rate; CDF: Cumulative distribution function; CE-OFDM: Constant envelope orthogonal frequency division multiplexing; CNR: Carrier-to-noise ratio; CP: Cyclic prefix; CPM: Continuous phase modulation; DFT: Discrete Fourier transformation; FDE: Frequency-domain equalization; HPA: High power amplifier; ICI: Inter-carrier interference; IDFT: Inverse discrete Fourier transform; IOV: Internet of Vehicles; ISI: Inter-symbol interference; ISM: Industrial scientific and medical; LTE: Long-Term Evolution; MMSE: Minimum mean-squared error; OFDM: Orthogonal frequency division multiplexing; PAM: Pulse amplitude modulation; PAPR: Peak-to-average power ratio; PDF: Probability density function; PO: Phase offset; PSD: Power spectral density; QAM: Quadrature

amplitude modulation; QPSK: Quadrature phase shift keying; RadCom: Radar and wireless communication; RMS: Root mean square; SER: Symbol error rate; SNR: Signal-to-noise ratio

**Funding**

This work is jointly supported by the MOST Program of International S&T Cooperation (Grant No.2016YFE0123200), National Natural Science Foundation of China (Grant No.61471100/61701503/61750110527), Science and Technology on Electronic Information Control Laboratory (Grant No.6142105040103), and Fundamental Research Funds for the Central Universities (Grant No.ZYGX2015J012).

**Authors' contributions**

YH, SH, and SM conceived the proposed scheme. QL and DH conducted the detailed derivation to evaluate the performance of the proposed scheme and wrote the manuscript. YG and RS reviewed the manuscript. All authors have read and approved the final manuscript.

**Competing interests**

The authors declare that they have no competing interests.

**Publisher's Note**

Springer Nature remains neutral with regard to jurisdictional claims in published maps and institutional affiliations.

**Author details**

<sup>1</sup>University of Electronic Science and Technology of China, Chengdu, China. <sup>2</sup>National Laboratory for Information Science and Technology, Tsinghua University, Beijing, China. <sup>3</sup>China Defense Science and Technology

Information Center, Beijing, China. <sup>4</sup>Science and Technology on Electronic Information Control Lab, Chengdu, China.

Received: 26 October 2017 Accepted: 18 April 2018

Published online: 04 May 2018

## References

- C Sturm, W Wiesbeck, Waveform design and signal processing aspects for fusion of wireless communications and radar sensing. *Proc. IEEE* **99**(7), 1236–1259 (2011).
- YL Sit, W Wiesbeck, C Sturm, et al., *The OFDM Joint Radar-Communication System: An Overview* (The Third International Conference on Advances in Satellite and Space Communications, Budapest, 2011), pp. 17–22.
- C Sturm, T Zwick, W Wiesbeck, *An OFDM System Concept For Joint Radar And Communications Operations* (IEEE 69th Vehicular Technology Conference, Vtc Spring 2009, Barcelona, 2009), pp. 26–29.
- S Hu, G Bi, YL Guan, et al., TDCS-based cognitive radio networks with multiuser interference avoidance. *IEEE Trans. Commun.* **61**(12), 4828–4835 (2013).
- S Hu, Z Liu, YL Guan, et al., Sequence design for cognitive CDMA communications under arbitrary spectrum hole constraint. *IEEE J. Sel. Areas Commun.* **32**(11), 1974–1986 (2014).
- S Hu, H Guo, C Jin, et al., Frequency-domain oversampling for cognitive CDMA systems: enabling robust and massive multiple access for Internet of Things. *IEEE Access* **4**, 4583–4589 (2016).
- M Krondorf, G Fettweis, OFDM link performance analysis under various receiver impairments. *EURASIP J. Wirel. Commun. Netw.* **2008**(1), 1–11 (2008).
- SK Chronopoulos, V Christofilakis, G Tatsis, et al., Performance of turbo coded OFDM under the presence of various noise types. *Wirel. Pers. Commun.* **87**(4), 1319–1336 (2016).
- SK Chronopoulos, G Tatsis, P Kostarakis, Turbo coded OFDM with large number of subcarriers. *J. Signal Inf. Process.* **3**(2), 161–168 (2012).
- S Hu, Z Liu, YL Guan, et al., Training sequence design for efficient channel estimation in MIMO-FBMC systems. *IEEE Access* **5**, 4747–4758 (2017).
- P Banelli, G Baruffa, S Cacopardi, Effects of HPA nonlinearity on frequency multiplexed OFDM signals. *IEEE Trans. Broadcast.* **47**(2), 123–136 (2001).
- JH Wen, SH Lee, YF Huang, et al., A suboptimal PTS algorithm based on particle swarm optimization technique for PAPR reduction in OFDM systems. *EURASIP J. Wirel. Commun. Netw.* **2008**(1), 1–8 (2008).
- SK Chronopoulos, G Tatsis, V Raptis, et al., Enhanced PAPR in OFDM without deteriorating BER performance. *Int. J. Commun. Netw. Syst. Sci.* **4**(3), 164–169 (2011).
- H Boche, B Farrell, PAPR and the density of information bearing signals in OFDM. *EURASIP J. Adv. Signal Process.* **2011**(1), 1–9 (2011). <https://doi.org/10.1155/2011/561356>.
- SK Chronopoulos, V Christofilakis, G Tatsis, et al., Reducing peak-to-average power ratio of a turbo coded OFDM. *Wirel. Eng. Technol.* **3**(4), 195–202 (2012).
- D Dardari, V Tralli, A Vaccari, A theoretical characterization of nonlinear distortion effects in OFDM systems. *IEEE Trans. Commun.* **48**(10), 1755–1764 (2014).
- Y Tsai, G Zhang, JL Pan, *Orthogonal Frequency Division Multiplexing with Phase Modulation and Constant Envelope Design* (2005 IEEE Conference on Military Communications, Atlantic City, 2005), pp. 17–20.
- SC Thompson, AU Ahmed, JG Proakis, et al., Constant envelope OFDM. *IEEE Trans. Commun.* **56**(8), 1300–1312 (2008).
- C Sturm, E Pancera, T Zwick, et al., *A Novel Approach to OFDM Radar Processing* (IEEE Radar Conference, Pasadena, 2009), pp. 4–8.
- C Sturm, M Braun, T Zwick, et al., *A Multiple Target Doppler Estimation Algorithm for OFDM Based Intelligent Radar Systems* (2010 European Radar Conference (EuRAD), Paris, 2010), p. 30.
- C Sturm, T Zwick, W Wiesbeck, et al., *Performance verification of symbol-based OFDM radar processing* (IEEE Radar Conference, Arlington, 2010), pp. 10–14.
- T Tsao, M Slamani, P Varshney, et al., Ambiguity function for a bistatic radar. *IEEE Trans. Aerosp. Electron. Syst.* **33**(3), 1041–1051 (1997).
- JG Proakis, *Digital Communications*, 4th edn. (McGraw Hill, New York, 2001), pp. 719–720.
- SC Thompson, AU Ahmed, JG Proakis, et al., *Constant Envelope OFDM Phase Modulation: Spectral Containment, Signal Space Properties and Performance* (2004 IEEE Conference on Military Communications, Monterey, 2004), p. 31.
- P Banelli, Theoretical analysis and performance of OFDM signals in nonlinear fading channels. *IEEE Trans. Wirel. Commun.* **2**(2), 284–293 (2003).
- AU Ahmed, SC Thompson, JR Zeidler, *Channel Estimation and Equalization for CE-OFDM in Multipath Fading Channels* (2008 IEEE Conference on Military Communications, San Diego, 2009), pp. 16–19.
- SC Thompson, JG Proakis, JR Zeidler, et al., *Constant Envelope OFDM in Multipath Rayleigh Fading Channels* (2006 IEEE Conference on Military Communications, Washington, DC, 2006), pp. 23–25.
- JG Proakis, M Salehi, *Communication Systems Engineering* (Prentice Hall, New Jersey, 1994), pp. 340–343.
- K Cho, D Yoon, On the general BER expression of one- and two-dimensional amplitude modulations. *IEEE Trans. Commun.* **50**(7), 1074–1080 (2002).
- J Zhu, J Wang, Y Huang, et al., On optimal power allocation for downlink non-orthogonal multiple access systems. *IEEE J. Sel. Areas Commun.* **35**(12), 2744–2757 (2017). <https://doi.org/10.1109/JSAC.2017.2725618>.
- S He, Y Huang, L Yang, et al., Coordinated multicell multiuser precoding for maximizing weighted sum energy efficiency. *IEEE Trans. Signal Process.* **62**(3), 741–751 (2014).
- Q Du, H Song, X Zhu, Social-feature enabled communications among devices towards smart IoT community. *IEEE Communications Magazine*. (2018).
- H Gacanan, F Adachi, On channel estimation for OFDM/TDM using MMSE-FDE in a fast fading channel. *EURASIP J. Wirel. Commun. Netw.* **1**, 53–56 (2009).
- I Kalet, The multitone channel. *IEEE Trans. Commun.* **37**(2), 119–124 (1989).
- N Levanon, *Radar Principles* (1988), pp. 39–67.

Submit your manuscript to a SpringerOpen<sup>®</sup> journal and benefit from:

- Convenient online submission
- Rigorous peer review
- Open access: articles freely available online
- High visibility within the field
- Retaining the copyright to your article

Submit your next manuscript at ► [springeropen.com](http://springeropen.com)